Calculation of the Darcy friction factor in a periodic tube bundle by means of wall-resolved large eddy simulations at bulk Reynolds number of 40,000

Pierre-Emmanuel Angeli

CALCULATION OF THE DARCY FRICTION FACTOR IN A PERIODIC TUBE BUNDLE BY MEANS OF WALL-RESOLVED LARGE EDDY SIMULATIONS AT BULK REYNOLDS NUMBER OF 40,000

Pierre-Emmanuel Angeli
CEA, Service de Thermo-hydraulique et de Mécanique des Fluides, Université Paris-Saclay
Gif-sur-Yvette 91191, France
pierre-emmanuel.angeli@cea.fr

ABSTRACT

The knowledge and understanding of turbulent flows in tube bundles are of primary interest for the design of pressurized water reactors. In particular, the accurate prediction of the pressure drop coefficient steps into the closure relationships of component thermalhydraulics codes, but is often difficult to address by an experimental approach. Wall-modeled large eddy simulation (LES) has proven its benefit in providing useful insight on the average flow structure, such as the velocity distribution, secondary flow and pressure drop. However, the use of a wall function could be considered as questionable since it amounts to artificially placing the dimensionless velocity on the universal wall law. On the other hand, wall-resolved LES allows an accurate resolution of the whole boundary layer despite a high computational cost. In the present study, wall-resolved large eddy simulations of a tri-periodic subchannel without mixing grids are performed with the WALE subgrid-scale model at a bulk Reynolds number of 40,000. The main features of the average flow are extracted and analyzed. When the mesh size tends toward zero, the friction coefficient tends toward the value that would be produced by a direct numerical simulation (DNS). Consequently, the DNS friction coefficient is deduced from a series of LES performed on successively refined meshes, assuming that the discrepancy between the LES and DNS coefficients varies as a power of the mesh size. The computed DNS friction factor exhibits finally a good agreement with the correlation of Rehme and used in the FLICA4 subchannel code.

KEYWORDS
Large eddy simulation, Darcy friction factor, rod bundle, Pressurized Water Reactor, TrioCFD.

1. INTRODUCTION

The calculation of the flow in tube bundles of Pressurized Water Reactors (PWR) is the subject of numerous numerical and experimental studies, whose main objectives are to determine the flow structure [1, 2], pressure drop or heat exchange coefficient correlations [3, 4], or to calibrate turbulence models [5]. Most often, the numerical simulations are carried out with RANS or LES models [6, 7]. DNS is not yet feasible for true reactor conditions, but is beginning to be accessible at more moderate Reynolds numbers [8, 9]. Such fine CFD computations of subchannel flow may be an alternative way to investigate subchannel codes closure relationships, instead of time-consuming and expensive experiments. In the context of nuclear thermalhydraulics reactor studies and safety, the upscaling refers to the passage of local information at the fine scale, to a more macroscopic information that can inform correlations usable in component thermalhydraulic nuclear core codes, such as FLICA4 [10, 11], simulating phenomena at an intermediate scale. The upscaling procedure is based on the application of appropriately defined averaging operators, from solutions calculated by CFD. The advantage of CFD is that the solutions are accessible at any point and at any time, which gives a very rich information. Its main drawbacks are the computational costs and the dependence of the solutions on the model employed. In the present work, we propose to use CFD to determine the pressure

drop coefficient, also called the Darcy friction factor, in an infinite tube bundle without mixing grid. In duct flows, the regular friction coefficient and the Reynolds number can be usually correlated by a law under the form $\Lambda = a \times \mathrm{Re}_b^{-b}$ [12]. The calculations are performed with the LES approach on several refined meshes at a bulk Reynolds of $\mathrm{Re}_b = 40{,}000$. We can get rid of the model uncertainty by postulating a convergence law for the friction coefficient, and deducing the value that would give a true DNS without running a such expensive simulation. The paper is organized as follows: section 2 first describes the setup of numerical simulations in terms of flow conditions, governing equations, numerical methods and computational meshes. It is followed in section 3 by an analysis focusing on the instantaneous and mean flow structures, secondary flow, Kolmogorov scale and friction coefficient. Section 4 ends the article by some concluding remarks.

2. SIMULATION SETUP

2.1. Flow conditions

We consider the isothermal and incompressible turbulent flow through an infinite rod bundle with a square arrangement of the pins of radius R and a rod-to-rod gap e. The numerical study may be reduced to a periodic geometric unit as shown in Fig. 1a and Fig. 1b, usually refered to as a typical subchannel (TSC) in the component thermalhydraulics codes. The ratio of the pitch over the pin diameter, $1 + e/2R$ = 1.326, is representative for actual PWR assemblies. The mean flow is parallel to the rod walls, and the viscous friction is responsible for a pressure loss along the bundle. Denoting D_h the hydraulic diameter, L the height of the bundle, U_b the bulk velocity and ΔP the pressure difference between inlet and outlet, the Darcy (or regular) friction coefficient in the direction parallel to rods writes:

$$\Lambda = \frac{D_h}{L} \frac{\Delta P}{\frac{1}{2}\rho U_b^2} \,. \tag{1}$$

The Reynolds number of the flow is calculated as follows:

$$\mathrm{Re} = \frac{\rho U_b D_h}{\mu} \,. \tag{2}$$

All the calculations reported in the present study are at Re = 40,000 which produces computationally expensive simulations but remains achievable by large eddy simulation and even by direct numerical simulation, or at least in a very close future. The computational domain is a TSC with an axial extension of H and periodic boundary conditions in all directions.

A height of $H = 10\ D_h$ is chosen for the computational domain. This choice is assessed by examining the two-point correlation obtained from the velocity fluctuations of a precursor LES. Even if the third component is less perfectly decorrelated than two others, as shown in Fig. 2, using a height of $H = 10\ D_h$ is considered as a fair compromise between physical relevance and computational cost because it is a large enough domain to obtain sufficiently decorrelated fields

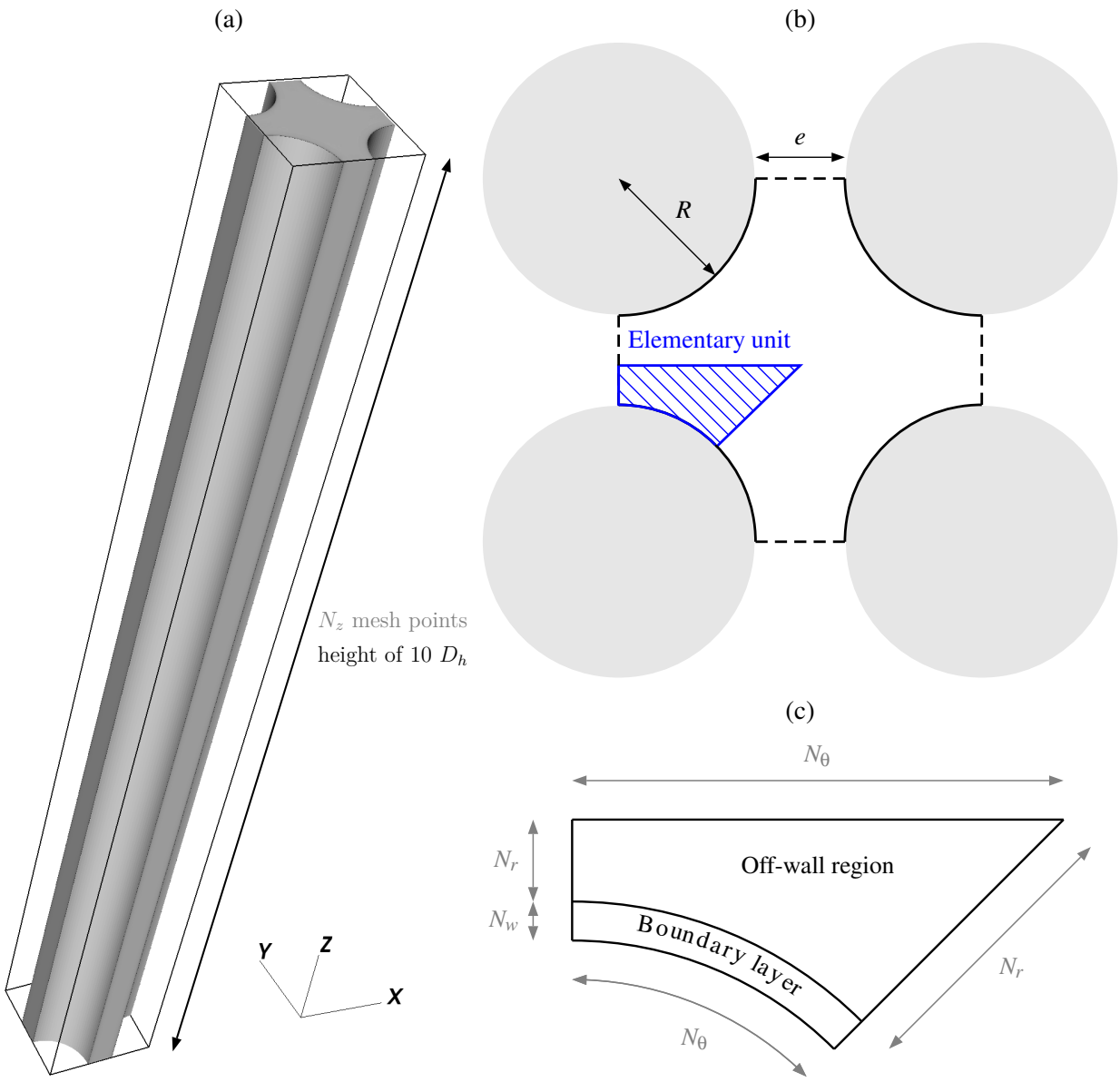

Figure 1. (a) computational fluid domain. (b) Top view of a typical subchannel. (c) Number of grid points in each direction of the symmetric elementary unit.

2.2. Governing equations

The LES approach combined with the WALE model for the subgrid-scale viscosity ν_{sgs} [13] is chosen. Denoting $\boldsymbol{u} = (u_1, u_2, u_3)$ the filtered velocity vector in the Cartesian frame of reference (x, y, z) shown in Fig. 1 whose origin is taken at the center of the subchannel, the governing equations are as follows, for $i = 1, 2, 3$:

$$\frac{\partial u_j}{\partial x_j} = 0\,, \tag{3}$$

$$\frac{\partial u_i}{\partial t} + u_j \frac{\partial u_i}{\partial x_j} = -\frac{1}{\rho}\frac{\partial p}{\partial x_i} + \frac{\partial}{\partial x_j}\left[\left(\nu + \nu_{\text{sgs}}\right)\left(\frac{\partial u_i}{\partial x_j} + \frac{\partial u_j}{\partial x_i}\right)\right] + F_i\,. \tag{4}$$

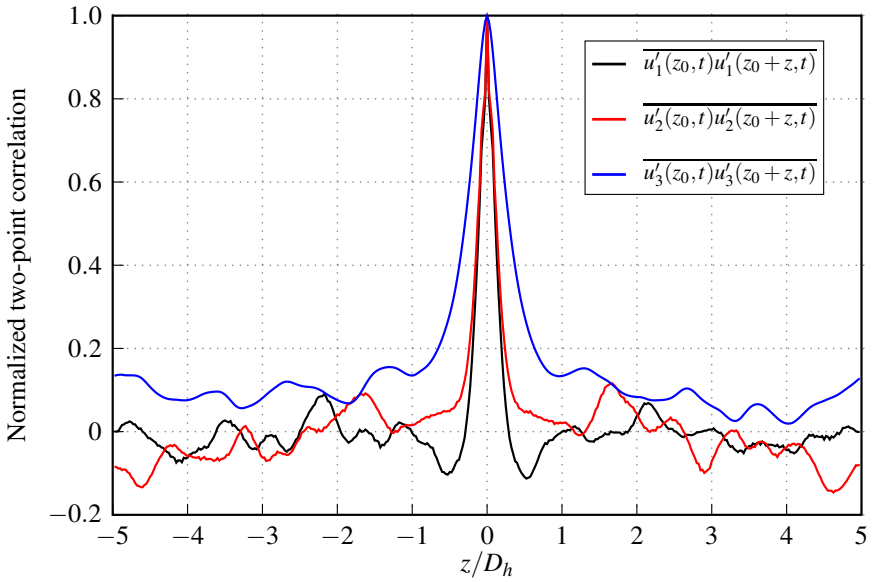

Figure 2. Two-point correlations of velocity fluctuations at the center z_0 of the subchannel.

Because of periodic conditions, the pressure loss ΔP in the axial direction is zero and is artificially reproduced by a forcing term $\boldsymbol{F} = (0, 0, F)$ added in the momentum balance equation (4). The initial flow rate $Q_0 = U_b \times S_{\text{TSC}}$, where $S_{\text{TSC}} = (2R + e)^2 - \pi R^2$ is the section of the TSC, is maintained all along the simulation through the penalization effect of the driving force $\boldsymbol{F}$.

2.3. Numerical methods

The numerical simulations are conducted with the open-source software TrioCFD of the CEA [14]. It uses a Finite Volume Element discretization method requiring tetrahedral meshes where the velocity unknowns are located at the center of faces, resulting in a total number of degrees of freedom being the number of faces, *i.e.* approximately twice the number of tetrahedra. Control volumes associated to each face of the mesh are built, forming a dual mesh. Similarly to the finite volume method, the momentum conservation equation is integrated on the primal cells, and the mass conservation equation on the dual cells. Fluxes and differential operators are computed using finite element approximations, finally providing a matrix system to be solved. The diffusion and convection operators are approximated using second order center and stabilized second order schemes, respectively. The temporal integration is made through the explicit Adams-Bashforth two-step method. A local time step is computed locally, corresponding to an average of the diffusion and convection time steps. The simulations being inescapably constrained by the very small diffusive time step compared to the convective one, a procedure of implicitation of the diffusive term is adopted. Thus the global time step used is the one resulting from the CFL condition, which ensures both numerical stability and a significant saving in computation time.

2.4. Computational meshes

The meshes are built from the symmetric elementary unit of the subchannel. The boundary layer and off-wall region are discretized separately, respectively with $N_\theta \times N_w$ and $N_\theta \times N_r$ points uniformly distributed as indicated in Fig. 1c, in a Cartesian manner. The obtained surface mesh is converted into a triangular

mesh extruded in the z-direction over $N_z - 1$ layers, generating prisms which are subsequently divided into tetrahedral elements. In order to investigate the mesh sensitivity of the numerical solutions, a series of four meshes is generated. For all of them, we take care to preserve a dimensionless wall distance y^+ close to a target value of 0.5. Such near-wall refinement is sufficient to avoid the use of a wall model, which leads to simulations called "wall-resolved". This procedure for mesh generation leads to a uniform size decrease of roughly $1.5^3 = 3.375$ between a mesh and the consecutive finer one. The properties of the resulting meshes are gathered in Table I, and an overview of the mesh shape is provided in Fig. 3

Table I. Properties of the meshes.

Mesh number	1	2	3	4
N_r	6	10	24	20
N_θ	14	20	32	50
N_w	14	20	26	36
N_z	401	601	901	1351
Tetrahedra	4,504,032	15,347,136	50,946,144	171,587,808
Δ_{min} [m]	4.4840e-05	3.5522e-05	2.6693e-05	2.0217e-05
Δ_{max} [m]	2.5633e-04	1.7372e-04	1.2296e-04	7.5614e-05
Δ_{avg} [m]	1.6947e-04	1.0838e-04	7.1878e-05	4.6932e-05
y^+	0.364	0.394	0.421	0.442

3. RESULTS AND DISCUSSION

3.1. Instantaneous flow

In every simulation, it is observed that the flow goes through a more or less long transient laminar phase, followed by a turbulent transition during which the flow becomes suddenly fully unsteady, chaotic and three-dimensional. Fig. 4 shows the normalized instantaneous axial velocity component for each mesh in a section of the subchannel at any time in the turbulent phase. As expected, the finer the mesh is, the more spatial scales are captured. Mesh 4 appears to be fine enough that it is hardly possible to distinguish the footprint of the meshes, giving a very smooth image of the numerical solution.

3.2. Time- and space-averaged flow

Owing to periodic conditions and invariant geometry in z direction, the time-averaged solutions are theoretically z-independent. They also exhibit symmetry properties following that of the geometric unit, which can be used to obtain a mean flow closer to the exact solution, *i.e.* averaged over an infinitely long time. Consequently, the instantaneous fields are averaged both temporally and spatially. At the time this article is

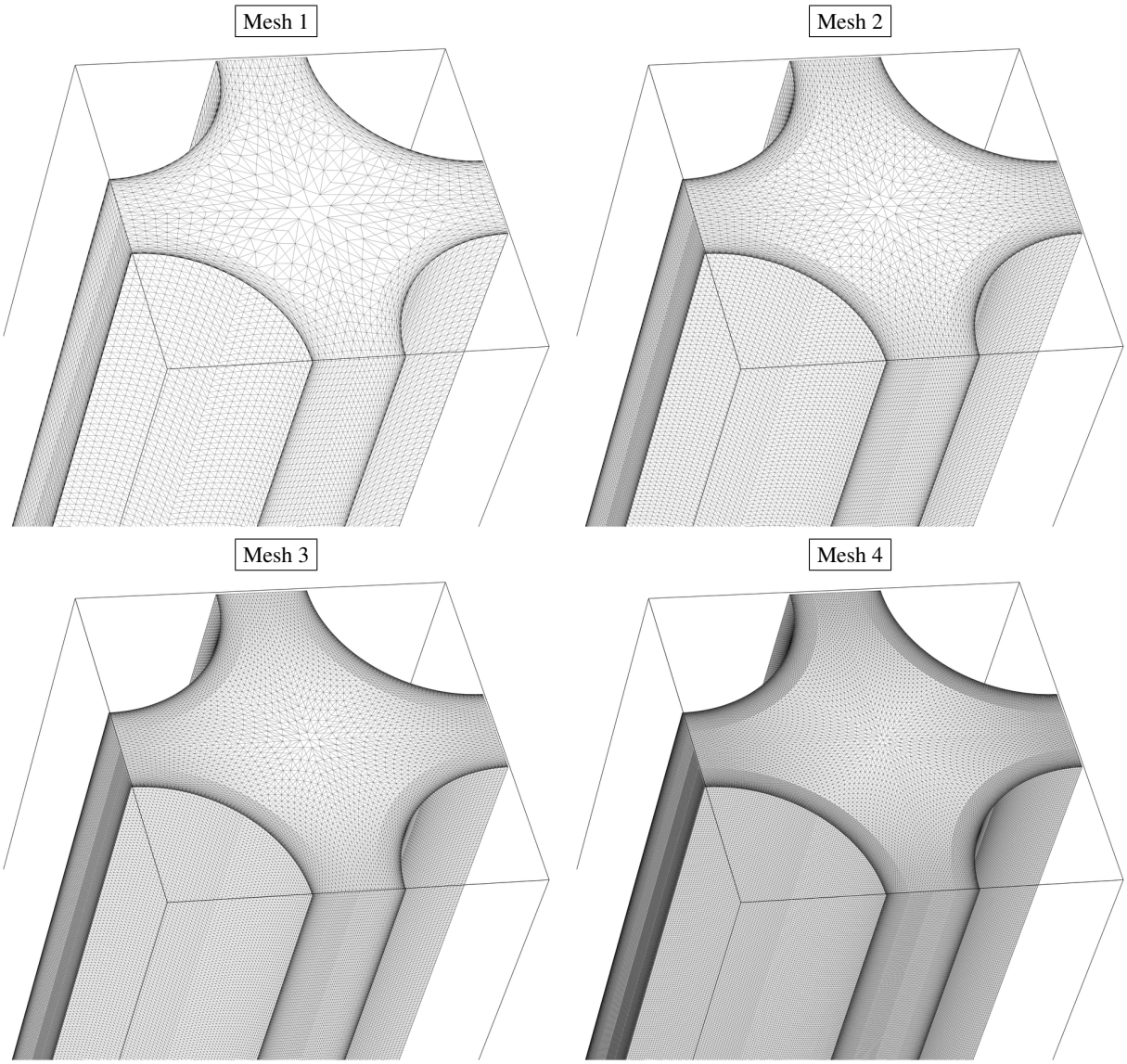

Figure 3. Overview of the computational meshes.

written, the first three simulations have been averaged over only 6 flow-through times, from the beginning of the turbulent phase. This is however sufficient to extract at least the significant first order mean flow features. Following the symmetry principle, the flow is also averaged over the eight symmetric elementary units. This amounts to considering the eight elementary cells as eight independent numerical experiments. Fig. 5 and Fig. 6 provide some visualizations of the mean axial velocity component averaged according to the previous procedure, as well as several profiles across the subchannel section. They reveal that the mean flow seems to converge towards a solution when the mesh is refined, which was expected.

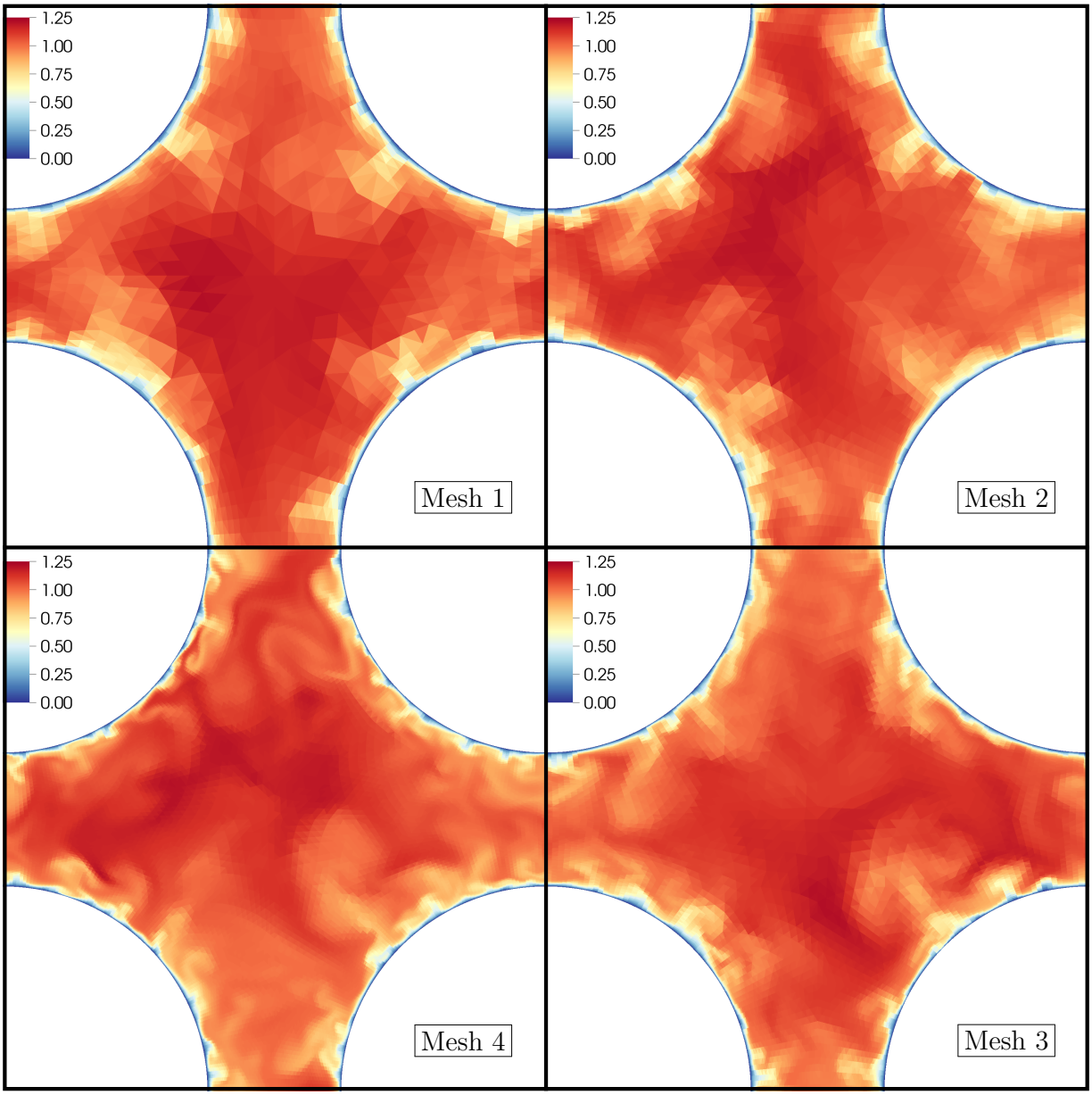

Figure 4. Instantaneous axial velocity component normalized with the bulk velocity U_b.

Interestingly, the non-dimensional velocity profiles plotted in Fig. 7 indicate that the mean flow follows the viscous sublayer law near the wall, and then joins up with the logarithmic sublayer. The length of the logarithmic sublayer is greater along the diagonal profile than between the two pins due the lack of space in the gap, but both would naturally increase with the Reynolds number. This constitutes an important element of validation of the simulations, because it shows that the fundamental behavior of near-wall turbulent flows is well captured.

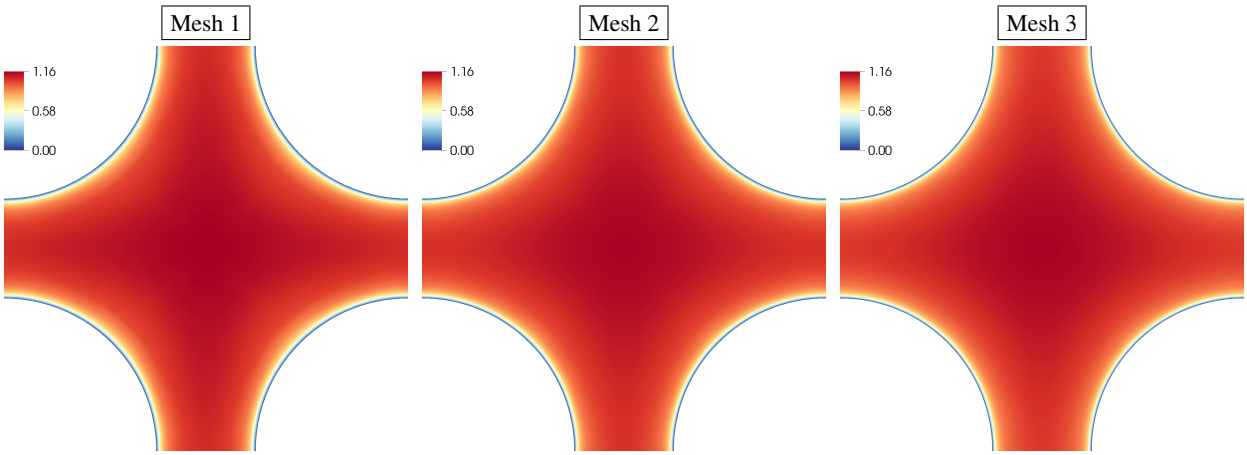

Figure 5. Averaged axial velocity component normalized with the bulk velocity U_b.

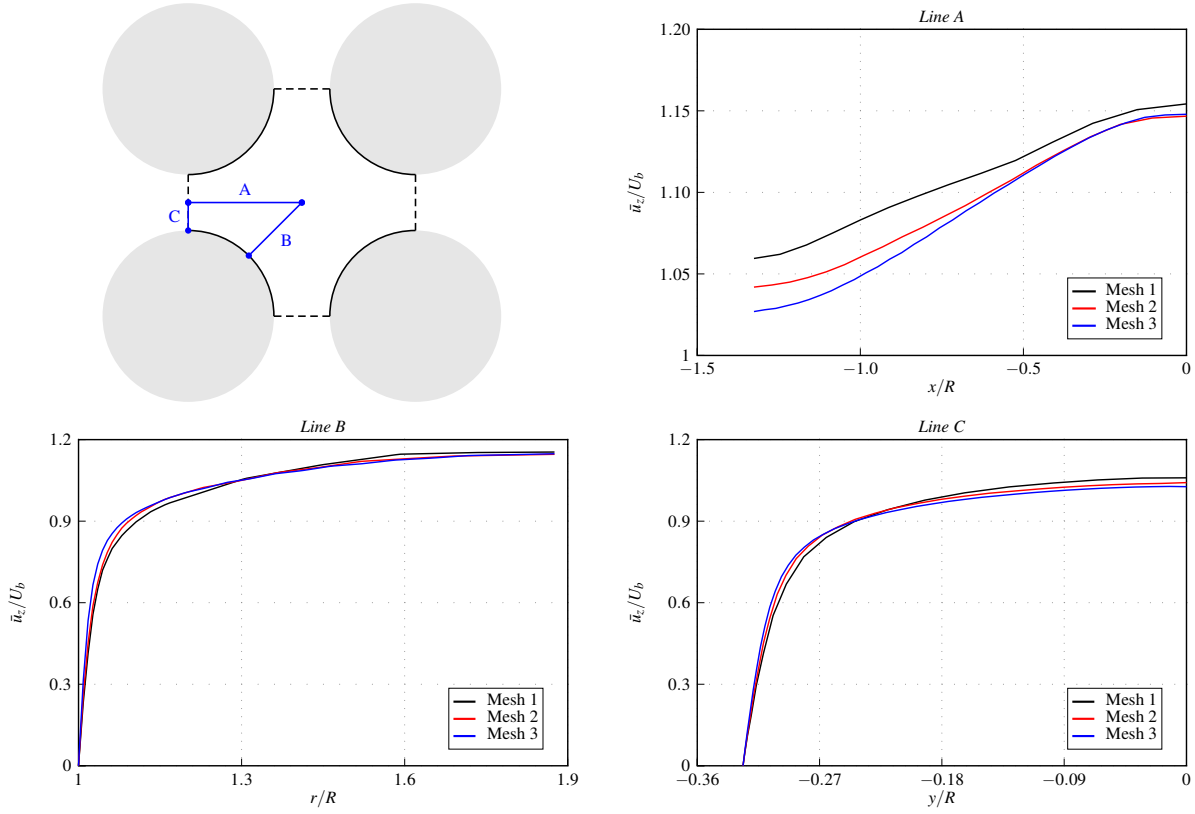

Figure 6. Normalized mean axial velocity component along various lines in the subchannel section.

3.3. Secondary flow

The secondary flow of second kind refers to as an organized structure of the mean transverse velocity observed for turbulent flows in non-circular ducts caused by the anisotropy of the Reynolds stress tensor [15, 16]. This phenomenon has been experimentally investigated for rod bundle, *e.g.* in [17]. In the present simulations, secondary flow can be clearly highlighted according to Fig. 8. Their maximum intensity is found to be around 0.5% of the bulk velocity, being of same order of magnitude but slightly lower

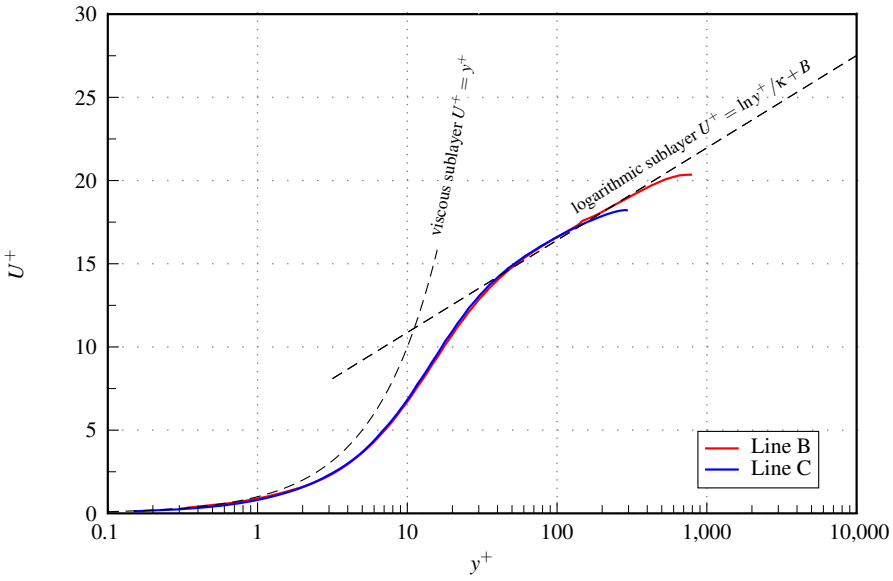

Figure 7. Semi-log plot of the axial velocity normalized using the friction velocity along the lines B and C of Fig. 6, for Mesh 3. Here we use $\kappa = 0.415$ and $B = 5.32$.

than the value computed in [9].

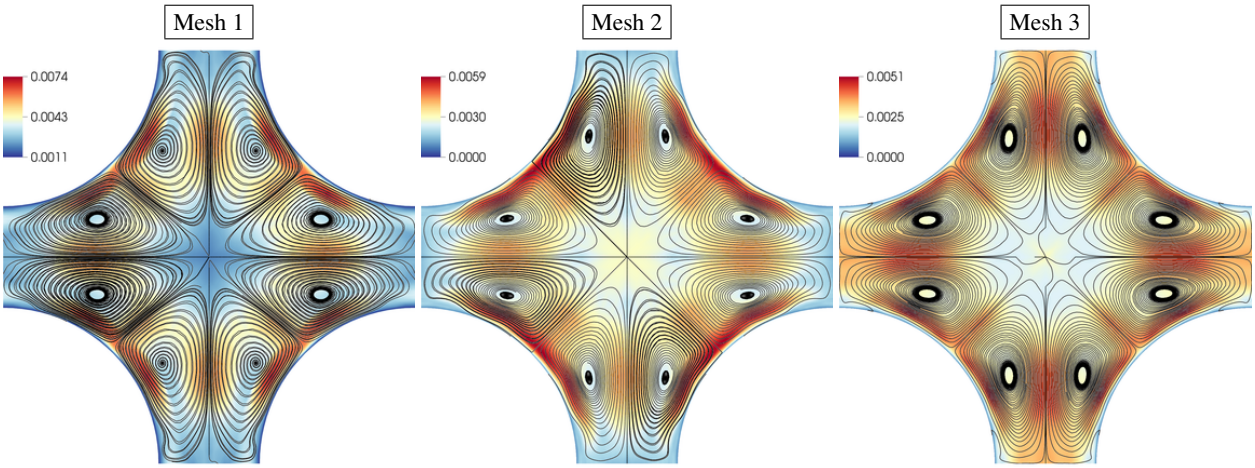

Figure 8. Top view of the secondary flow in the subchannel section. The streamlines are superimposed with a color map showing the norm of transverse velocity normalized with the bulk velocity U_b.

As shown in Fig. 9, the secondary flow is composed of eight counter-rotating vortices, alternating. Their direction of rotation in each of the eight cells is opposite to that of the two adjacent cells. Their intensity is maximal close to the rod wall and at $\theta \approx 65°$ in the polar coordinate system represented in Fig. 9.

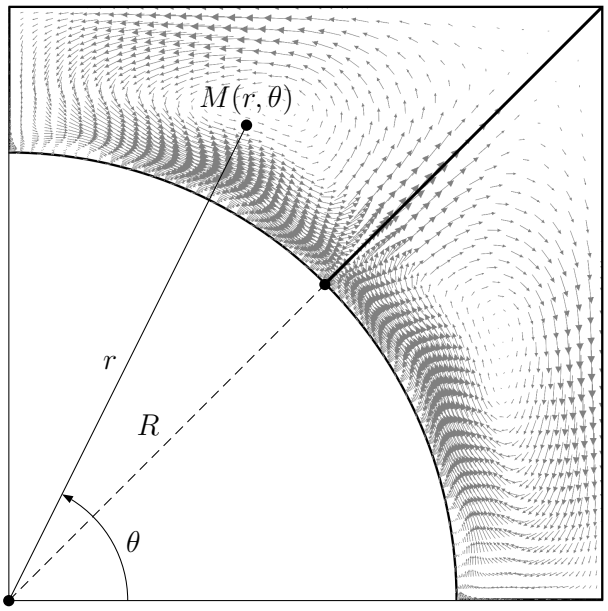

Figure 9. Top view of the transverse velocity vectors scaled by magnitude for the mesh 3. A polar frame is defined in order to compute the location of the maximum transverse velocity.

Table II. Value and location of the maximum transverse velocity in the polar frame of reference represented in Fig. 9.

Mesh number	1	2	3
Value (% of U_b)	0.741	0.593	0.506
Radial position r/R	1.082	1.058	1.076
Angular position θ [°]	58.85	49.74	65.32

3.4. Assessment of mesh size compared to the Kolmogorov scale

The Kolmogorov scale is the smallest eddy size that can exist in the flow, the smaller vortices being instantly dissipated by the molecular viscosity. It can be estimated as:

$$\eta_K = \left(\frac{\nu^3}{\varepsilon}\right)^{1/4} . \tag{5}$$

A true DNS would require that the mesh size is lower or equal than η_K. Fig. 10 gives the local mesh size Δ, computed as the mesh volume to the power $1/3$, normalized by the Kolmogorov scale computed by LES. The meshes under consideration are obviously not suitable for a DNS. Nevetherless the refinement factor of 1.5 between consecutive meshes is appproximately recovered, and a rough estimation indicates that a sixth mesh of 2 billions of tetrahedra would be of sufficient size for a DNS. Such a simulation is currently in progress.

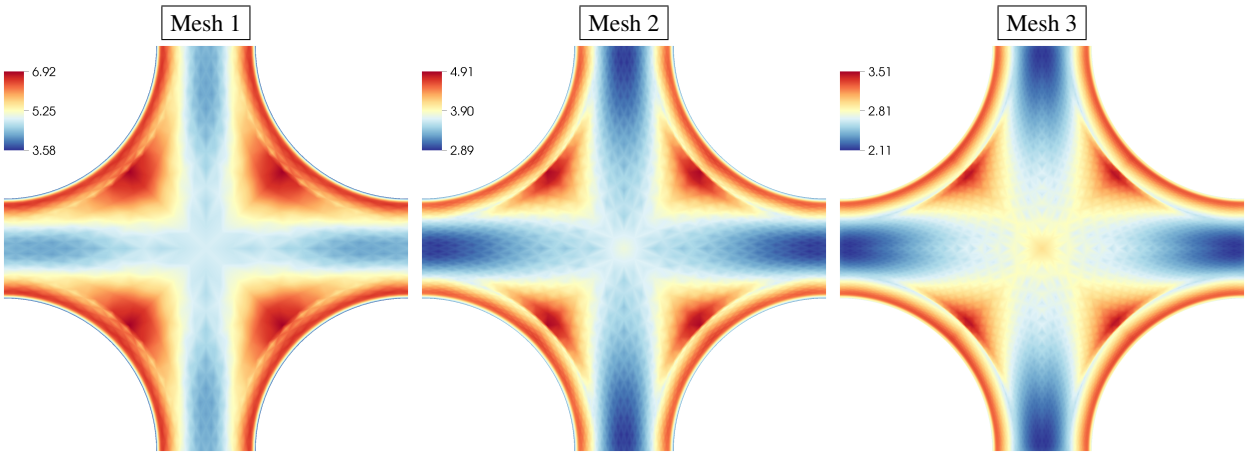

Figure 10. Ratio of the mesh size over the Kolmogorov scale.

3.5. Darcy friction factor

As ΔP is zero, equation (1) has to be adapted. The balance equation of momentum in the axis direction gives the real pressure loss:

$$\Delta P = \frac{F_v}{S_{\text{TSC}}} \tag{6}$$

where the viscous stress on rod walls writes:

$$F_v = \left(\iint_{\text{walls}} -\mu \nabla \boldsymbol{u} \cdot \boldsymbol{n} dS \right) \cdot \boldsymbol{e}_z \,. \tag{7}$$

Then, the postprocessing of F_v yields the regular friction coefficient:

$$\Lambda = \frac{D_h}{L} \frac{F_v}{\frac{1}{2}\rho S_{\text{TSC}} U_b^2} \,. \tag{8}$$

The time evolution of Λ is plotted in Fig. 11a, and its time-averaged version in Fig. 11b. As this coefficient is space-integrated over the wall surface, it appears to converge quickly to a nearly constant value.

One postulates that if the mesh size Δ is small enough, then the pressure drop coefficient converges according to the following law:

$$|\Lambda_\Delta - \Lambda_{\Delta \to 0}| = a \Delta^b \,, \tag{9}$$

where $\Lambda_{\Delta \to 0}$ is the asymptotic value which would arise from a DNS. The previous equation (9) is the Richardson extrapolation truncated at first order and gives the apparent order of convergence b. The absolute value is added because a non-monotonic convergence is likely to happen [18], which is finally not the case here. The numerical value of $\Lambda_{\Delta \to 0}$ can be hardly computed, but can be obtained by an indirect procedure. If at least three simulations, *i.e.* three pairs $(\Delta_i, \Lambda_{\Delta_i})$, are available then the unknowns $(a, b, \Lambda_{\Delta \to 0})$ of equation (9) can be numerically calculated. This methodology has already been successfully employed with the same code to compute the turbulent kinetic energy [19]. Applied to meshes $i = 2$, 3 and 4, the numerical

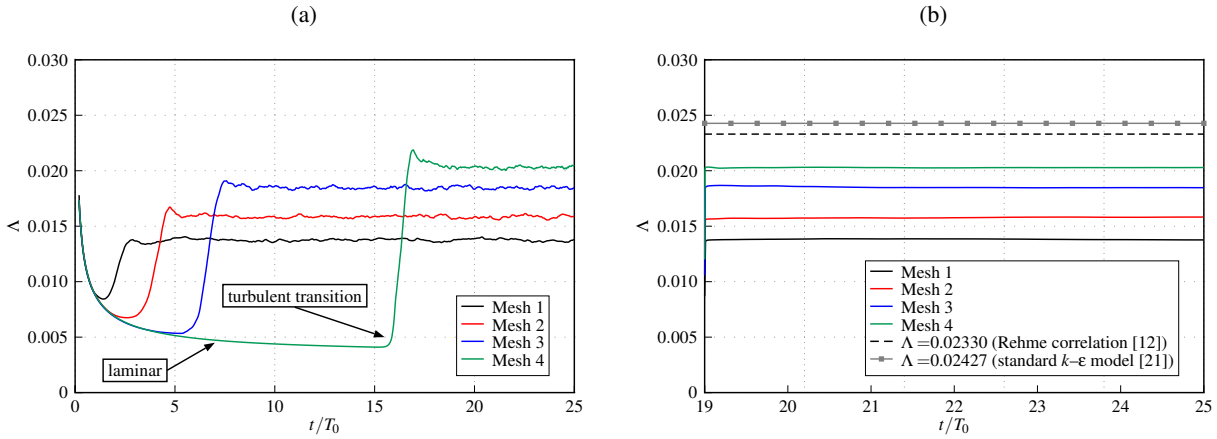

Figure 11. (a) Temporal evolution of the friction factor. (b) Time-averaged evolution of the friction factor. The abscissa is normalized by the flow-through time $T_0 = H/U_b$.

resolution yields

$$\begin{cases} \Lambda_{\Delta\to 0} &= 0.02375\,, \\ a &= 66.76\,, \\ b &= 0.99\,. \end{cases} \tag{10}$$

It can be noted that the order of convergence $b = 0.99$ is in very good agreement with the expected value $b = 1$, which in the considered numerical method is the order of convergence of the velocity gradient involved in the equation (7) [20]. The computed value $\Lambda_{\Delta\to 0}$ is very consistent with $\Lambda = 0.02330$ obtained with the Rehme correlation $\Lambda = 0.194 \times \mathrm{Re}_b^{-0.2}$ [12] and with $\Lambda = 0.02427$ obtained with the standard k–ε model [21], both shown in Fig. 11b, since the relative discrepancy is respectively of +1.93% and -2.14%. The solution (10) is graphically represented in Fig. 12. It turns out that very fine meshes are required in order to obtain a decent accuracy on the Darcy friction factor: the relative discrepancy between the value on mesh 4 and the DNS value $\Lambda_{\Delta\to 0}$ is of 15%.

4. CONCLUSIONS

In this study, the incompressible and isothermal turbulent flow at bulk Reynolds of 40,000 in an infinite rod bundle has been numerically investigated using wall-resolved large eddy simulations on successively refined meshes. The instantaneous flow has been spatially and temporally averaged, which highlighted an organized mean flow structure. The normalized near-wall velocity was found to satisfy the universal wall law. The existence of secondary flow formed by eight recirculating cells has been demonstrated. The primary goal of this work was to compute accurately the regular friction coefficient by deducing from several LES the value that would arise from an "infinitely" refined mesh, *i.e.* the DNS value. The apparent order of convergence of the friction coefficient with respect to the mesh size towards the DNS value is found to be close to unity, matching the convergence order of the velocity gradient in the numerical method used. Finally, the value of the friction coefficient is in very good agreement with the correlation of Rehme and with that calculated with the RANS k–ε model combined with a wall law. More complete results and analyses will be presented in a forthcoming publication, including especially new simulations up to four billion of degrees of freedom almost meeting the mesh requirements for a DNS.

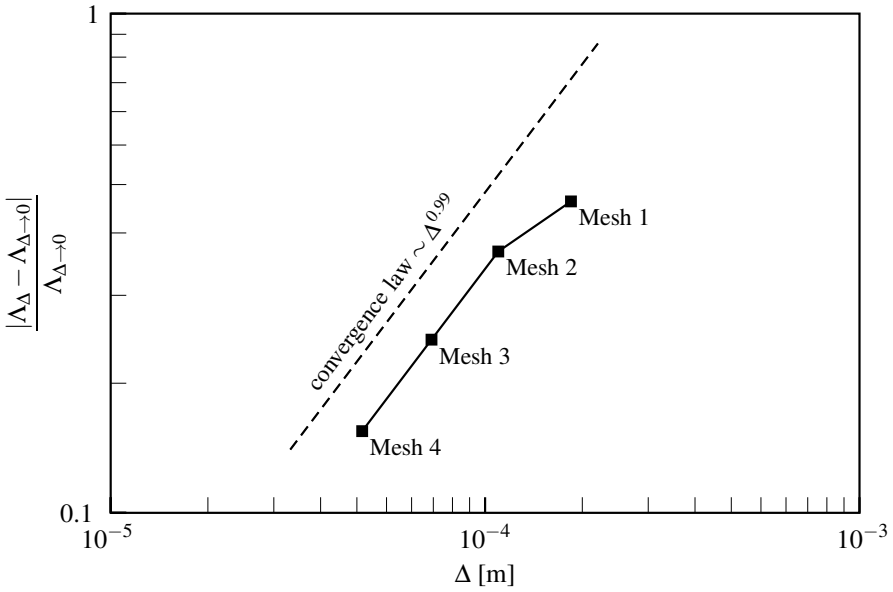

Figure 12. Log-log plot of the relative discrepancy between the friction coefficients computed by LES on mesh size Δ and by DNS. With $\Lambda_{\Delta\to 0} = 0.02375$, the points for meshes 2, 3 and 4 are aligned on a straight line of slope 0.99.

ACKNOWLEDGMENTS

This work was granted access to the HPC resources of TGCC under the allocation 2020-A0092A10460 attributed by GENCI (Grand Équipement National de Calcul Intensif). The author would like to acknowledge the support received from the TRUST platform team, for the help on carrying out large calculations on the TGCC clusters, and especially Anida Khizar for the use of the Medcoupling library of the SALOME plateform.

REFERENCES

1. S. Kim, B. Jeon, H.-S. Choi, D.-J. Euh, and S.-K. Moon, "Experimental visualization of flow structure inside subchannels of a 4 x 6 rod-bundle," *Ann. Nucl. Energy*, **140**, pp. 107097 (2020)

2. X. Li et al., "Experimental study of transient friction characteristics and velocity distribution of pulsatile flow in rod bundles," *Ann. Nucl. Energy*, **140**, pp. 107124 (2020)

3. Z. Ma et al., "Friction and local pressure loss characteristics of a 5 x 5 rod bundle with spacer grids," *Ann. Nucl. Energy*, **140**, pp. 107106 (2020)

4. J. Li, Y. Xiao, H. Gu, D. Liu, and Q. Zhang, "Development of a correlation for mixed convection heat transfer in rod bundles," *Ann. Nucl. Energy*, **155**, pp. 108151 (2021)

5. E. Baglietto, H. Ninokata, and T. Misawa, "CFD and DNS methologies development for fuel bundle simulations," *Nucl. Eng. Des.*, **236**, pp. 1503–1510 (2006)

6. H. Wang, D. Lu, and Y. Liu, "PIV measurement and CFD analysis of the turbulent flow in a 3 x 3 rod bundle," *Ann. Nucl. Energy*, **140**, pp. 107135 (2020)

7. H. Wang, S. Wang, and D. Lu, "Turbulent flow of water in a 3 x 3 rod bundle – Numerical results from RANS, URANS and LES," *Prog. Nucl. Energy*, **129**, pp. 103516 (2020)

8. A. Shams and T. Kwiatkowski, "Towards the Direct Numerical Simulation of a closely-spaced bare rod bundle," *Ann. Nucl. Energy*, **121**, pp. 146–161 (2018)

9. A. Kraus, E. Merzari, T. Norddine, O. Marin, and S. Benhamadouche, "Direct numerical simulation of fluid flow in a 5x5 square rod bundle," *Int. J. Heat Fluid Flow*, **90**, pp. 108833 (2021)

10. S. Aniel et al., "FLICA4: Status of Numerical and Physical Models and Overview of Applications," *Proc. 11th International Topical Meeting on Nuclear Reactor Thermalhydraulics (NURETH-11)*, Avignon, France, (2-6 October, 2005)

11. P. Raymond, B. Spindler, and R. Lenain, "FLICA4: Status of Numerical and Physical Models and Overview of Applications," *Nucl. Eng. Des.*, **124**, pp. 299–313 (1990)

12. K. Rehme, "Pressure drop correlations for fuel element spacers," *Nucl. Technol.*, **17**, pp. 15–23 (1973)

13. F. Nicoud and F. Ducros, "Subgrid-scale stress modelling based on the square of the velocity gradient tensor," *Flow Turbul. Combust.*, **62**, pp. 183–200 (1999)

14. P.-E. Angeli, "Overview of the TrioCFD Code: Main Features, V&V Procedures and Typical Applications to Nuclear Engineering," *Proc. 16th International Topical Meeting on Nuclear Reactor Thermalhydraulics (NURETH-16)*, Chicago, USA, (2015)

15. C. Speziale, "On nonlinear K–l and K–ε models of turbulence," *J. Fluid Mech.*, **178**, pp. 459–475 (1987)

16. R. Vinuesa, P. Schlatter, and H. Nagib, "Secondary flow in turbulent ducts with increasing aspect ratios," *Phys. Rev. Fluids*, **3**, pp. 054606 (2018)

17. V. Vonka, "Measurement of secondary flow vortices in a rod bundle," *Nucl. Eng. Des.*, **106**, pp. 191–207 (1988)

18. I. Celik, Z. Cehreli, and I. Yavuz, "Index of Resolution Quality for Large Eddy Simulations," *J. Fluids Eng.*, **127**, pp. 949–958 (2005)

19. P.-E. Angeli, "Verification and validation of LES of a triple parallel jet flow in the context of a thermal striping study," *Nucl. Eng. Des.*, **353** (2019)

20. P.-E. Angeli, A. Puscas, G. Fauchet, and A. Cartalade, "FVCA8 Benchmark for the Stokes and Navier-Stokes Equations with the TrioCFD Code – Benchmark Session," in *Finite Volumes for Complex Applications VIII – Methods and Theoretical Aspects*, edited by C. Cancès and P. Omnes, pp. 181–203, Springer, (2017)

21. P.-E. Angeli, A. Bergeron, and U. Bieder, "Toward an innovative CFD-based upscaling methodology to elaborate closures for the FLICA4 subchannel code," *Proc. International Topical Meeting on Advances in Thermal Hydraulics (ATH 2020)*, (2020)